RSC Advances

PAPER

View Article Online
View Journal | View Issue

Cite this: *RSC Adv.*, 2021, **11**, 6247

Terahertz spectral investigation of temperature induced polymorphic transformation of 2,2dinitroethylene-1,1-diamine

Liu Quancheng,[a] Zhang Qi,[b] Li Guilin,[a] Guo Zhicheng,[c] He Xiangyang,[a] Xie chai,[a] Deng Hu[a] and Shang Liping*[a]

Received 22nd December 2020
Accepted 29th January 2021

DOI: 10.1039/d0ra10754a

rsc.li/rsc-advances

The dynamic process of polymorphic transformations provides deep insights into the understanding of both the performance of explosives and its packing sensitivity. While terahertz spectroscopy is a sensitive tool that can be used to characterize its intermolecular forces. In this paper, terahertz time-domain spectroscopy (THz-TDS) is employed to investigate the polymorphic transformations of the explosive 2,2dinitroethylene-1,1-diamine (FOX-7) under a heating process. Solid-state density functional theory (DFT) uncovers the physical mechanisms that contribute to the polymorphic transformation. This is achieved by assessing the calculated spectra relative to the actual spectra from experiment. The results suggest that the THz spectral features that arise represent a redistribution of the intermolecular forces during the polymorphic transformations. This research will assist the understanding of the evolving properties of FOX-7, under external stimuli, which is vital knowledge for an explosive substance that can combust or detonate.

1 Introduction

Explosives are greatly important to both civil and military applications and, hence, have attracted worldwide interest over an extensive period of time.[1,2] Typically, an explosive can exist in two or more different crystalline forms, which is called polymorphism.[3] These polymorphs have the same chemical composition but exhibit different structures at the molecular, crystal, and interface levels, which results in a variety of energy, impact sensitivity and detonation properties.[3] Hence, for application purposes, it is necessary for an explosive to be maintained as a stable polymorph, thus enabling a reliable release of energy and its safety. Numerous researchers are presently focused on methods for the control of polymorphic transformations.[4–6]

It has been determined that phase transformations of a polymorphic explosive under external stimulus loading could be a necessary step before its final combustion or detonation.[7] The understanding of the polymorphic transformations of the explosive is indispensable for revealing its sensitivity mechanism. An explosive crystal undergoes many complex physical processes during its polymorphic transformations, which includes a change in the molecular structure, symmetries and molecular stacking patterns, *etc.* Usually, X-ray diffraction is adopted as the standard method for the study of polymorphic transformations,[8,9] which provides the geometric structure of the molecular crystal. However, this is difficult in the present circumstance since the polymorphic transformations involve a dynamic motion; this important factor reveals the performance and packing sensitivity of the crystalline explosive. Infrared[10] and Raman spectroscopy[11] could provide this dynamic observation for various different molecular structures. However, some polymorphic transformations produce minor distortions in the molecular structure, which creates difficulties for spectroscopy techniques of these types. Furthermore, recent research suggests that the molecular stacking patterns, which are highly dependent on the intermolecular forces, play an important role in the energy and safety of the explosives.[12] Hence, the investigation of any weak intermolecular interactions during the polymorphic transformations will greatly assist the understanding, prediction and control of this process.

Terahertz (referring to the frequency range from 0.1 to 10 THz.[13]) vibrational transitions are related to the weak interactions, such as intermolecular hydrogen bonding and van der Waals (vdW) forces, that dominate molecular packing geometries.[14] For our purposes, terahertz time-domain spectroscopy (THz-TDS) is claimed to be a sensitive tool for investigating polymorphic transformations. Despite THz spectral features of numerous energetic materials, including traditional explosives[15,16] and new ionic salts,[17,18] being widely reported, methods

[a]*School of Information Engineering, Southwest University of Science and Technology, Mianyang 621010, China. E-mail: shangliping@swust.edu.cn*

[b]*Institute of Chemical Materials, China Academy of Engineering Physics, Mianyang 621900, China*

[c]*School of Defense Science and Technology, Southwest University of Science and Technology, Mianyang 621010, China*

to determine the characteristics of the polymorphic transformation process urgently need development.

2,2Dinitroethylene-1,1-diamine (FOX-7)[19,20] is a relatively novel explosive that is currently attracting substantial interest since, in comparison to cyclotrimethylenetrinitramine (RDX), it has the superior advantages of high density, excellent detonation performance and low sensitivity. Under elevated temperatures, FOX-7 crystals are observed to experience a α to β to γ structural change before its chemical decomposition. Moreover, the molecular arrangement of the FOX-7 crystals are in the form of wave-shaped layers, which results in extensive intermolecular forces that act both within and between the layers.[7] These features enable FOX-7 to be a suitable substance for the verification of THz spectral sensitivity. In this paper, we produce the THz spectra of FOX-7 under a heat induced process. Furthermore, an understanding of the specific vibrations in the THz region, calculated *via* density functional theory (DFT), provides insights into the mechanism of the polymorphic transformations.

2 Materials and experimental setup

2.1 Sample preparation

FOX-7 powder is prepared by the institute of chemical materials, China Academy of Engineering Physics. The synthetic route is mainly based upon the nitration of 4,6-dihydroxy-2-methylpyrimidine in a mixed acid at a low temperature.[21] To lessen the particle scattering effects as a spectral feature,[22] the FOX-7 crystals are lightly grinded to minimize the particle size to within 74 μm. Generally, explosives exhibit strong absorption in the THz band, which limits the effective dynamic range[23] (DR) of the spectra. One widely adopted method to counter this is to mix a small amount of explosive powder with matrix materials, which helps to form a stable pellet that avoids the saturated absorption.[18,24] Teflon is advantageous in this regard since it has a low absorption[25] and a high melting point (above 260 °C). In this paper, 40 mg of FOX-7 powder is mixed with 500 mg of Teflon powder (with a particle size of 5 μm), which are then compressed into a pellet (with 13 mm diameter and 1.89 mm thickness) under a pressure of 2 tons (Atlas, Specac). Before the spectral measurement, the pellet is stored in a dry environment for 24 hours to release the internal pressure.

2.2 Experimental setup

The experimental configuration for this work is plotted in Fig. 1. In brief, a femtosecond laser (MaiTai SP, Spectra-Physics) with a central wavelength of 800 nm, a pulse width of 80 fs and a repetition rate of 80 MHz is employed for the energy supply. The power of the pump and probe lasers are 100 mW and 20 mW, respectively. The pump laser is focused onto the gap (200 μm) of a dipole photoconductive antenna (Zomega, America) with a lens (focal length = 5 mm) to produce THz waves. Then, the generated THz waves are collected with a Teflon lens (focal length = 50 mm) and focused into a spot with diameter approximately equal to 6 mm (focal length = 150 mm). The THz

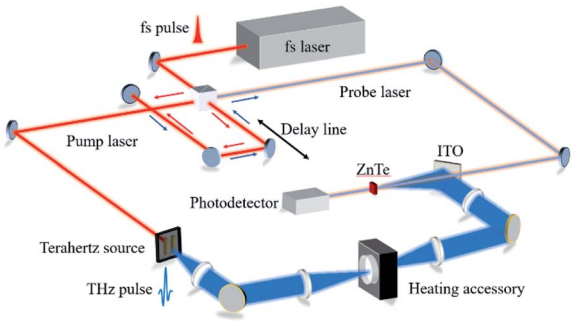

Fig. 1 A sketch of the set-up for terahertz time-domain spectroscopy.

waves that pass through the sample are transmitted using a symmetrical configuration. Meanwhile, the probe laser is guided through an optical delay, and it is finally collected simultaneously with the THz waves. The coherent detection is implemented using a ZnTe (110) crystal (with a thickness of 2 mm) and an optical balanced detector (Zomega, America). The photovoltage measured by the detector is proportional to the electric field of the THz waves. In this configuration, the bandwidth[23] of the dry air is approximately 2.5 THz, and the spectra resolution[23] is 17 GHz, as plotted in Fig. 2.

A heating accessory, supplied by PIKE TECHNOLOGIES (USA), is employed for the heating process. The pellet is inserted into the heating accessory and positioned at the focal point to ensure that no THz waves are obscured. The actual temperature of the pellet is calibrated using a T-type thermocouple (JK7000, China Jinke Co., Ltd) supplied by the local quality supervision bureau. The probe of thermocouple is fixed onto the edge of the pellet using a high temperature-resistance pastern (YK-8909, China Yikun Rubber Co., Ltd). To reduce the effects of water vapor interference on the spectra, dry air produced by the combination of an air compressors (JB-2000, China Nantong jinjuba Machinery Co., Ltd), a refrigeration dryer (RD-8, China Hangzhou Tianyuan Co., Ltd) and a heatless dryer (TYWD-0.3, China Hangzhou Tianyuan Co., Ltd) is continually pumped into the THz-TDS system. All the measurements are implemented within the relative humidity of 0%.

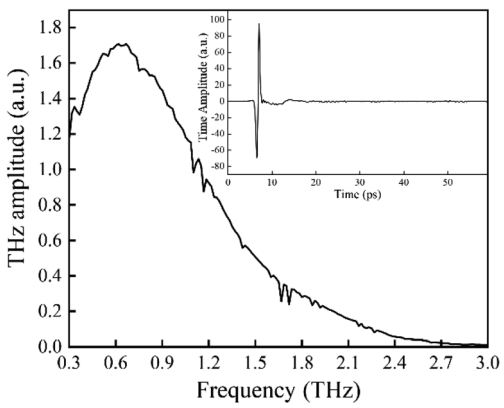

Fig. 2 Frequency spectra of dry air in this experimental configuration. The thumbnail represents the time domain spectra.

2.3 Extraction of absorption coefficient

In the THz measurements, the time-domain signal ($E(t)$) is recorded by changing the relative delay time between the pump and the probe laser. Subsequently, $E(t)$ is converted to a frequency spectrum, $E(\omega)$, *via* fast Fourier transform (Origin 2018, OriginLab). The absorption coefficient, $\alpha(\omega)$, of the pellet can be evaluated as follows:[26]

$$T(\omega) = \frac{E_{\text{sam}}(\omega)}{E_{\text{ref}}(\omega)} = \rho(\omega)\exp(-j\varphi(\omega)), \quad (1)$$

$$n(\omega) = 1 + \frac{\varphi(\omega)c}{\omega d}, \quad (2)$$

$$\alpha(\omega) = \frac{2}{d}\ln\left(\frac{4n(\omega)}{\rho(\omega)[n(\omega)+1]^2}\right), \quad (3)$$

where the subscripts sam and ref represent the sample and air, respectively. Moreover, $n(\omega)$ is the refractive index, c is the speed of light in air and d is the thickness of the sample.

2.4 DFT calculations

Solid state DFT calculations are implemented using a CASTEP program as a part of the Material studio package (Accelrys). The generalized gradient approximation (GGA)-Perdew–Burke–Ernzerhof (PBE) function is adopted for the geometry optimization and the vibrational calculations. To better account for the forces relating to noncovalent bonding, which are extraordinarily important for these low frequency vibrational modes, the Grimme semi-empirical dispersion-corrections are included in these calculations. The quality of the energy calculations is ultra-fine. The energy cut-off is set at 830 eV, and the SCF tolerance is $5.0 \times e^{-7}$ eV per atom. The crystalline structures of α, β and γ-FOX-7 are obtained as given in previous reports.[27,28]

3 Results and discussions

3.1 THz absorption spectra

Firstly, under a heating process from 21.5 to 111.8 °C, the THz spectra of FOX-7 are record as plotted in Fig. 3(a). At 21.5 °C, FOX-7 exhibits two absorption bands centred at 1.58 and 2.20 THz. As the temperature increases from 21.5 °C, the two absorption bands display intensity attenuations and they are red shifted in frequency. Such variations could be ascribed to anharmonicity effect[29,30] that is caused by the thermal expansion of the FOX-7 crystals. The increase of the crystalline geometry sizes with temperature gradually weakens the intermolecular forces, eventually producing THz vibrational modes that have lower energies and frequencies. However, the degree of the two frequency shifts differ significantly. Specially, in the region from 21.5 to 101.5 °C, the frequency shift of 2.20 THz is 0.12 THz in contrast to a shift of 0.06 THz for the 1.58 THz band. This suggests a different temperature dependency for the modes that produce these two absorptions. As the temperature rises to 101.5 °C, an absorption increase is observed within the region of 0.3 to 1.8 THz. This phenomenon becomes increasingly significantly for enhanced heating times and higher temperatures. As heating reaches 111.8 °C, no further changes are observed in the absorption spectra, which indicates that the crystal is temporarily in a stable state. Here, two absorption bands emerge at 1.13 and 1.69 THz, while the 1.58 THz feature disappears and the 2.20 THz absorption band at 25 °C shifts to 2.02 THz. These significant variations of the absorption features suggest that, in this region, the FOX-7 undergoes a polymorphic transformation.

Moreover, we also record the spectra under a cooling process as plotted in Fig. 3(b). The two absorption bands of 1.13 THz

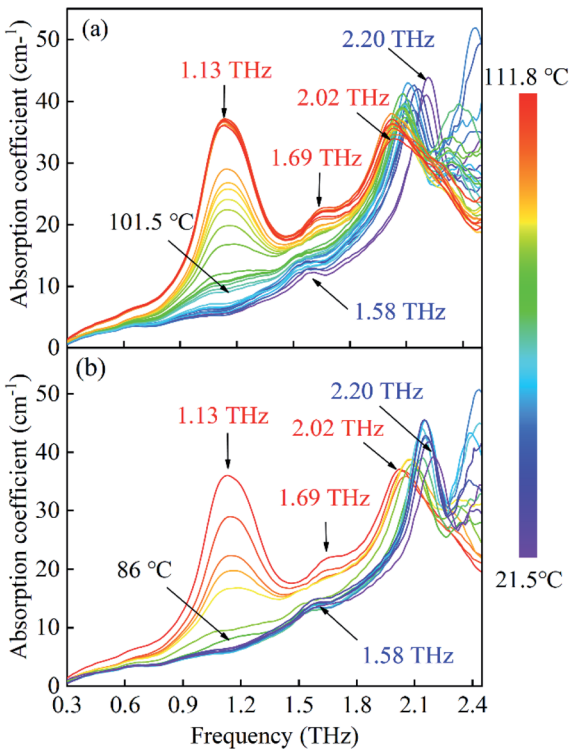

Fig. 3 The evolution of the absorption spectra of FOX-7 with a heat cycling ranging from 21.5 to 111.8 °C. (a) Heating process, (b) cooling process.

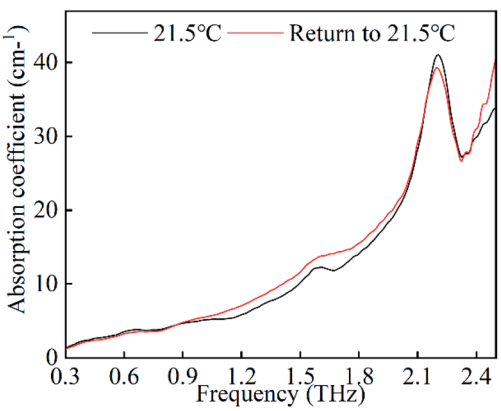

Fig. 4 A comparison of the absorption spectra of FOX-7 after heat cycling from 21.5 to 111.8 °C.

and 1.69 THz exhibit intensity decreases, which finally disappear after approximately 15 minutes, while the 1.58 THz absorption band is later re-observed. In addition, the 2.03 THz absorption band displays a blue shift for this process. Next, we compare the spectra of FOX-7 (taken at room temperature) after the temperature is cycled; this is plotted in Fig. 4. We can see that the two spectra show the same absorption positions and a slight difference in the absorption intensity. In general, explosive crystals that undergo high temperature cycling typically experience intermolecular damage, due to the anisotropic expansion with a preferred orientation. The same absorption positions indicate that the FOX-7 crystals remain stable when temperature cycling under the heating process.

Furthermore, the spectra of FOX-7 are investigated for temperatures from 128.2 to 222.7 °C as plotted in Fig. 5(a). In this situation, the 1.13 THz absorption band experiences the remarkable variations shown in Fig. 5(b). In the region of 128.2 to 170.3 °C, the 1.13 THz absorption band shows intensity attenuation due to the thermal expansion. Above 175.5 °C, the absorption exhibits an increase in intensity and it is blue shifted in frequency. At 189.2 °C, the absorption finally shifts to 1.26 THz. As mentioned above, the heating process always results in a red shift in the frequency. This blue shift on increasing the temperature suggests a transition in the intermolecular forces. Hence, the newly generated 1.26 THz is considered as a representation of the second polymorphic transformation. From

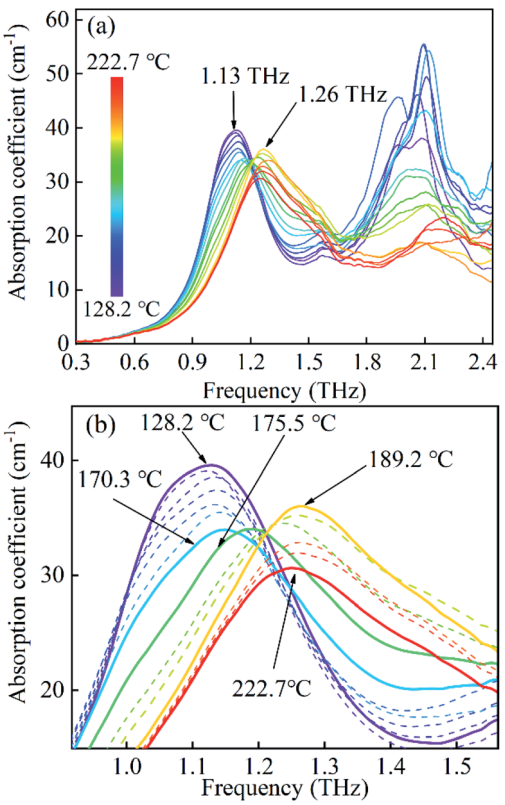

Fig. 5 (a) The evolution of the absorption spectra of FOX-7 under the heating process from 128.2 to 222.7 °C. (b) The spectra magnified in the 1.0 to 1.4 THz region.

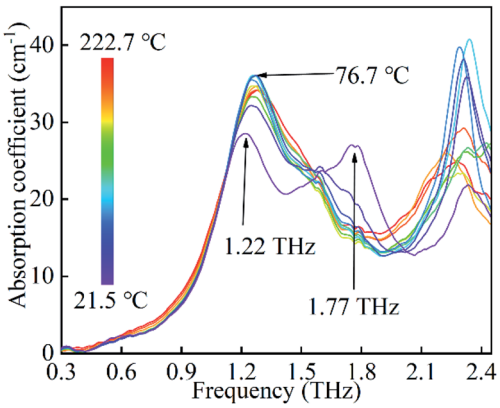

Fig. 6 The evolution of the absorption spectra of FOX-7 under the cooling process from 222.7 to 21.5 °C.

189.2 to 222.7 °C, the absorption shows intensity attenuation and red shifting. This response to the temperature, as shown by the spectra, indicates that the FOX-7 crystal is within a stable state in this region. In addition, the absorption features around 2.03 THz seem to experience intensity attenuations and blue shifts toward the high frequency. Due to the limitation of the low DR and the (signal to noise ratio) SNR, the detailed characteristics are unable to be identified.

Finally, the spectra of the cooling process from 222.7 to 21.5 °C are recorded as plotted in Fig. 6. In this process, the spectra have slight instabilities in the absorption positions and intensities, which indicate the crystals of FOX-7 undergo

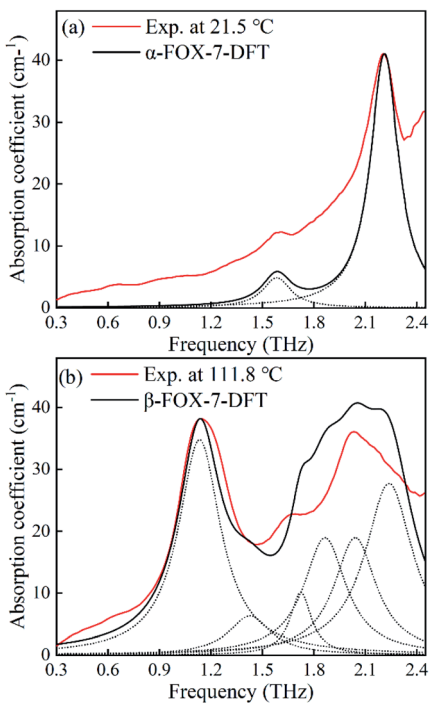

Fig. 7 Comparison of the experimental and the DFT-based spectra of (a) α-FOX-7 and (b) β-FOX-7. The dashed lines represent each calculated mode.

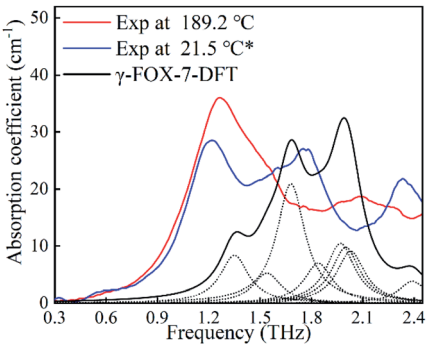

Fig. 8 Comparisons of the experimental and the DFT-based spectra of γ-FOX-7. The dash line represents each vibrational mode. The asterisk indicates the temperature cycling from 222.7 to 21.5 °C.

a disordered state. As temperature decreases from 76.7 to 21.5 °C, the 1.26 THz absorption band exhibits intensity attenuation and red shifts. This suggests that the crystals are unstable and undergo structural transformations. At room temperature, two notable absorption bands emerge at 1.22 and 1.77 THz. Obviously, the spectra at room temperature are significantly different after this heat cycling, which suggests that the FOX-7 crystals experience an irreversible damage in this case.

3.2 DFT calculations

In this section, DFT calculations are employed to determine the origin of the variations in the spectra. Fig. 7 and 8 are plots that compare the experimental and simulated results. For α-FOX-7, the DFT-based spectra contain two vibrational modes centred at 1.59 and 2.21 THz, which are in good agreement with the experimental absorption spectra at 21.5 °C. At 1.59 THz, the intensities in the simulated spectra are underestimated, possibly due to the neglect of the scattering effects of the powder. In addition, the DFT spectra of β-FOX-7 mainly exhibit six strong vibrational modes in this region. The calculated mode at 1.13 THz is also a good representation of the experimental 1.13 THz absorption at 111.8 °C. However, the 1.69 THz absorption is overestimated and relates to the calculated mode at 1.73 THz. While the experimental spectra exhibit only one absorption at 2.05 THz, the DFT calculations, in contrast, provides three vibrational modes. There are two possible reasons for this difference: (1) the DFT calculations generally overestimate phonon modes in comparison to experimental spectra at a harmonic limit.[13,30,31] (2) The generated 1.13 and 1.69 THz peaks produce strong absorption band, which sharply decrease the DR near 2 THz. This could result in an incomplete detection of the absorption features in this band.[23] Overall, the DFT calculations of α- and β-FOX-7 appropriately replicate the experimental spectra at 21.5 and 111.8 °C. This also proves that the variations in the observed absorption spectra at 101.5 °C are attributed to a α to β transformation.

Now examining the cooling process from 222.7 to 21.5 °C, the irregular spectra evolution indicates that the FOX-7 crystals undergo various unstable states. In this situation, the positions

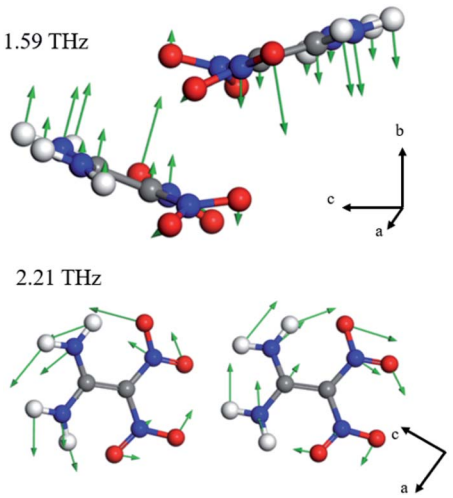

Fig. 9 Depiction of the 1.59 and 2.21 THz vibrational modes. The red, blue, grey and white spheres represent the oxygen, nitrogen, carbon and hydrogen atoms, respectively. The green arrows denote the displacement of each atom.

of the atoms in the crystal unit cell could vary hugely with temperature. The unit cell of the γ-FOX-7 that is adopted for the DFT calculations is recorded by single crystal X-ray diffraction after quenching to −73 °C.[28] This could explain the possible reason for the appreciable deviation between the experimental spectra and the DFT calculations, which is shown in Fig. 8. However, the newly evolved absorption of 1.26 THz at 189.2 °C is an appropriate reproduction of the calculated mode at 1.32 THz. The DFT calculations may also provide appropriate insights into the spectral feature that relates to the absorption band at 1.13 THz gradually shifting to 1.26 THz from 128.2 to 189.2 °C.

Material studio provides the visual insights into the origins of the vibrational modes that are based on the displacement of each atom of the crystal. Fig. 9 is a plot of the 1.59 and 2.21 THz modes that dominate the absorption features of FOX-7 at room temperature. For 1.59 THz, the atoms principally translate along the positive direction of the *b*-axis with the neighbouring atoms moving in the opposing direction; this originates from the vdW interactions between the layers. In contrast, the 2.21

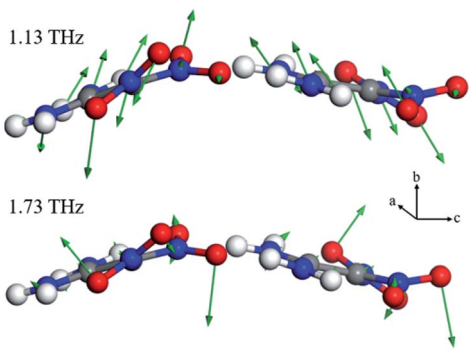

Fig. 10 Depiction of the 1.13 and 1.69 THz vibrational modes.

THz modes exhibit rotations about their centres-of-mass within the *a–c* plane, which derives from their interactions *via* the hydrogen bonding networks in the plane. The heating process weakens these intermolecular forces, which results in a red shifting of the absorption frequency. The degree of the shift of the two modes indicates that the *b*-axis has a weaker expansion coefficient compared to the *a–c* plane. Moreover, the disappearance of 1.59 THz mode during the transformation from α to β suggests that a weakening of the vdW forces between layers is an essential component of the transformation.

For the β-polymorph, the modes of primary interest are 1.13 and 1.69 THz for an examination of the α to β transformation. As shown in Fig. 10, the four oxygen atoms of the two nitro groups deviate from the molecular plane, which produces molecular asymmetry. Moreover, the deviated oxygen atoms also reconstruct the hydrogen bonding networks with neighbouring amino groups. These vibrational variations produce new modes that are mainly in the form of libration; these variations are responsible for the 1.13 and 1.69 THz absorption bands. Moreover, only two oxygen atoms clearly participate in the calculated 1.71 THz mode, and hence result in a weaker absorption intensity.

For the spectral evolution of the heating process in the region of 128.2 to 189.2 °C, the 1.13 THz absorption successively shifts to 1.26 THz. This suggests that the newly generated 1.26 THz absorption originates from similar libration. One explanation for this phenomenon, in which the same vibrational mode produces different absorption features, is a lattice rearrangement of the FOX-7 crystals. Fig. 11 is a plot of the vibrational mode that can be identified as the origin of the experimental absorption at 1.26 THz. Clearly the vibrational mode is also in the form of libration. Moreover, due to the rearrangement of the lattice, the vibrational direction varies from the *b*-axis to the *a*-axis. In addition, it is observed that the unit cell of the γ-polymorph is formed of eight molecules in two conformations. The atoms in the two conformations exhibit dissimilar displacements, and hence provide different absorption intensities in the spectra.

The essence of the polymorphic transformations is that, with external stimuli, the crystal translates to a specific, more stable form. Under heating, the THz spectra of FOX-7 crystals response to variations in the intermolecular forces, which includes both vdW forces and hydrogen bonding. These low frequency vibrations provide microscale insights into understanding the evolutions of the polymorphic transformation. As stated earlier, it has been reported that the minor distortions to the α to β transformation are difficult to detect with Raman and IR spectroscopy.[10] In contrast, the THz technique is sensitive to such distortions. This proves that THz-TDS is potentially an important tool for accurate investigation of polymorphic transformations.

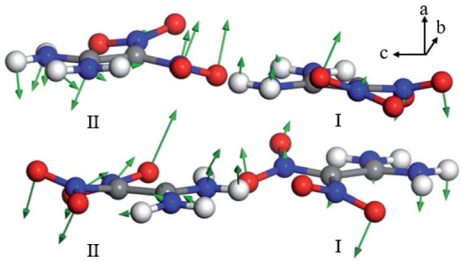

Fig. 11 Depiction of the 1.26 THz vibrational modes.

4 Conclusions

In this paper, we employ THz-TDS to investigate the explosive FOX-7 under a heating process over the range 0.3 to 2.4 THz. An α to β and β to γ transformation are identified at 101.5 and 175.5 °C, respectively. The spectral evolutions for α to β transformation include the disappearance of the 1.58 THz absorption band and two new absorption bands at 1.13 and 1.69 THz. Comparing with the DFT-based spectra, the origins of these changes are found to be related to a weakening of the vdW forces between the layers and a rearrangement of the hydrogen bonding networks within the layers. We also determine that the blue shifting of 1.13 THz to 1.26 THz represents a β to γ transformation, which represents a significant rearrangement of the crystalline lattice.

Conflicts of interest

There are no conflicts to declare.

Acknowledgements

This research was funded by the National Defense Basic Scientific Research Program of China (No. JCKY2018404C007, JSZL2017404A001, and JSZL2018204C002); Sichuan Province Science and Technology Support Program (No. 2019YFG0114; 2021YFG0253).

References

1 D. M. Badgujar, M. B. Talawar, S. N. Asthana and P. P. Mahulikar, *J. Hazard. Mater.*, 2008, **151**, 289–305.
2 J. J. Sabatini and K. D. Oyler, *Crystals*, 2016, **6**, 22.
3 R. Bu, H. Li and C. Zhang, *Cryst. Growth Des.*, 2020, **20**, 3561–3576.
4 Z. G. Ma, B. Gao, P. Wu, J. C. Shi, Z. Q. Qiao, Z. J. Yang, G. C. Yang, B. Huang and F. D. Nie, *RSC Adv.*, 2015, **5**, 21042–21049.
5 F. Y. Gong, J. H. Zhang, L. Ding, Z. J. Yang and X. B. Liu, *Chem. Eng. J.*, 2017, **309**, 140–150.
6 Z. J. Yang, L. Ding, P. Wu, Y. G. Liu, F. D. Nie and F. L. Huang, *Chem. Eng. J.*, 2015, **268**, 60–66.
7 R. Bu, W. Xie and C. Zhang, *J. Phys. Chem. C*, 2019, **123**, 16014–16022.
8 X. Zheng, S. Yu, W. Wen, Y. Wen, P. Wang, L. Lan, X. Dai, Y. Han, J. Li and Y. Li, *Propellants, Explos., Pyrotech.*, 2018, **43**, 1164–1170.
9 Y. Liu, S. C. Li, Z. S. Wang, J. J. Xu, J. Sun and H. Huang, *Cent. Eur. J. Energ. Mater.*, 2016, **13**, 1023–1037.

10 M. M. Bishop, N. Velisavljevic, R. Chellappa and Y. K. Vohra, *J. Phys. Chem. A*, 2015, **119**, 9739–9747.
11 Z. P. Lu, X. G. Xue, L. Y. Meng, Q. Zeng, Y. Chi, G. J. Fan, H. Z. Li, Z. M. Zhang, F. D. Nie and C. Y. Zhang, *J. Phys. Chem. C*, 2017, **121**, 8262–8271.
12 R. P. Bu, Y. Xiong, X. F. Wei, H. Z. Li and C. Y. Zhang, *Cryst. Growth Des.*, 2019, **19**, 5981–5997.
13 Z. Zhu, C. Cheng, C. Chang, G. Ren, J. Zhang, Y. Peng, J. Han and H. Zhao, *Analyst*, 2019, **144**, 2504–2510.
14 M. Takahashi, *Crystals*, 2014, **4**, 74–103.
15 J. Hooper, E. Mitchell, C. Konek and J. Wilkinson, *Chem. Phys. Lett.*, 2009, **467**, 309–312.
16 L. M. Lepodise, J. Horvat and R. A. Lewis, *J. Phys. Chem. A*, 2015, **119**, 263–270.
17 D. Ganesh, E. Narsimha Rao, M. Venkatesh, K. Nagarjuna, G. Vaitheeswaran, A. K. Sahoo and A. K. J. A. O. Chaudhary, *ACS Omega*, 2020, **5**, 2541–2551.
18 N. Palka, M. Szala and E. Czerwinska, *Appl. Opt.*, 2016, **55**, 4575–4583.
19 R. X. Xu, C. W. An, H. Huang, J. Y. Wang, B. Y. Ye and B. Liu, *RSC Adv.*, 2019, **9**, 21042–21049.
20 W. Z. Ma, Y. J. Yang, F. Q. Zhao, K. Z. Xu, J. K. Zhang, M. Zhang and Z. C. Feng, *RSC Adv.*, 2020, **10**, 1769–1775.
21 M. Anniyappan, M. B. Talawar, G. M. Gore, S. Venugopalan and B. R. Gandhe, *J. Hazard. Mater.*, 2006, **137**, 812–819.
22 H. L. Zhan, R. Chen, X. Y. Miao, Y. Z. Li, K. Zhao, S. J. Hao and X. H. Chen, *IEEE Trans. Terahertz Sci. Technol.*, 2018, **8**, 477–481.
23 W. Withayachumnankul and M. Naftaly, *J. Infrared, Millimeter, Terahertz Waves*, 2014, **35**, 610–637.
24 G. Damarla, M. Venkatesh and A. K. Chaudhary, *Appl. Opt.*, 2018, **57**, 8743–8750.
25 P. D. Cunningham, N. N. Valdes, F. A. Vallejo, L. M. Hayden, B. Polishak, X.-H. Zhou, J. Luo, A. K. Y. Jen, J. C. Williams and R. J. Twieg, *J. Appl. Phys.*, 2011, **109**, 043505.
26 T. D. Dorney, R. G. Baraniuk and D. M. J. J. A. Mittleman, *J. Opt. Soc. Am. A*, 2001, **18**, 1562–1571.
27 J. Evers, T. M. Klapotke, P. Mayer, G. Oehlinger and J. Welch, *Inorg. Chem.*, 2006, **45**, 4996–5007.
28 M. J. Crawford, J. Evers, M. Gobel, T. M. Klapotke, P. Mayer, G. Oehlinger and J. M. Welch, *Propellants, Explos., Pyrotech.*, 2007, **32**, 478–495.
29 S. Najmaei, Z. Liu, P. M. Ajayan and J. Lou, *Appl. Phys. Lett.*, 2012, 100.
30 Z. Wu, Z. Zhu, C. Cheng, J. Zhang, Y. Gong, M. Xu, S. Li and H. Zhao, *Spectrochim. Acta, Part A*, 2020, **225**, 117509–117517.
31 S. Zong, G. Ren, S. Li, B. Zhang, J. Zhang, W. Qi, J. Han and H. Zhao, *J. Mol. Struct.*, 2018, **1157**, 486–491.